applied optics

Geometrical-based quasi-aspheric surface description and design method for miniature, low-distortion, wide-angle camera lens

Zhenfeng Zhuang,[1,*] Xavier Dallaire,[1] Jocelyn Parent,[1] Patrice Roulet,[1] and Simon Thibault[1,2]

[1]Immervision Inc., 2020 Robert-Bourassa Blvd., Suite 2320, Montreal, Quebec H2A 2A5, Canada
[2]Centre d'optique, photonique et laser, Département de physique, de génie physique et d'optique, Université Laval, 2375, rue de la Terrasse, Québec G1V 0A6, Canada
*Corresponding author: zhenfeng.zhuang@immervision.com

Received 18 June 2020; revised 18 August 2020; accepted 19 August 2020; posted 20 August 2020 (Doc. ID 400528); published 18 September 2020

In addition to utilizing traditional aspheric surfaces, complicated geometric curves for meeting stringent design requirements can also be adopted in optical systems. In this paper, we investigate two geometric shape modeling schemes, namely, pedal and cosine curves, which allow for representation of an S-shaped profile for the optical design of a camera lens. To obtain a powerful tool for representing a quasi-aspheric surface (QAS) to resemble the designed form surface, we linearly combine the pedal/cosine function with a base conic section. The detailed parameterization process of representation is discussed in this paper. Subsequently, an existing starting point that has similar specifications to that of the design requirements is selected. During the optimization process, a least-squares fitting algorithm is implemented to obtain the optimal coefficient values of the proposed QAS representation, and then the parameters (radii, air thickness, lens thickness, coefficients, materials, etc.) of the optical system are set to optimize the optical performance, gradually aiming to minimize the predefined merit function. We demonstrate the applicability of the proposed geometric modeling schemes via two design examples. In comparison to a conventional aspheric camera lens of the same specifications, the optical performance with respect to field of view and distortion has been improved due to higher degrees of design freedom. We believe that the proposed technology of geometric modeling schemes promises to improve optical performance due to these higher degrees of freedom and appears to be applicable to many different camera lenses.

https://doi.org/10.1364/AO.400528

1. INTRODUCTION

Optical lens systems have become one of the most popular components in the growing market of consumer products, which play a vital role in our daily life as a function of taking photographs. Furthermore, the market demand for high-performance miniature optical lens systems has been increasing with the continuous progress of entertainment devices, wearables, portable electronic and medical devices [1–3], particularly smartphones, which are now used all around the world. Aiming to enhance the quality of the end-user experience, smart electronic devices integrated two, three, four or even more image-capturing components are gradually becoming mainstream products in the market. Thus, miniature optical lenses with various features have been developed in order to match the performance of complementary metal oxide semiconductor (CMOS) image sensors [4,5].

The optical lens systems are commonly composed of several optical elements that now can achieve extraordinary optical performance. Traditionally, the optical elements are represented by aspheric surfaces that must redirect rays from object space to image space as well as correct aberrations to produce the sharpest images possible. However, conventional optical lens systems with polynomial aspheric surfaces are not favorable for satisfying the stringent requirements of low f-number, large field of view (FoV), required chief ray angle, small distortion, and short total track length (TTL) simultaneously. Currently, design and improvement processes are becoming increasingly challenging as the pixels in CMOS image sensors shrink in size. Therefore, utilizing such surface descriptions is unable to satisfy the demands of current technology development [6]. A more effective surface representation, which has higher degrees of design freedom, is necessary in these applications [7–10].

Freeform optics has recently attracted increasing attention in nonimaging optical illumination system [11,12] and imaging optical system [13,14] applications by virtue of the fact that it gives higher degrees of freedom in optical design, as well as the flexibility of arbitrary surface shapes. The definition of a freeform surface varies in the literature. Generally, a freeform surface is defined as an optical surface without linear or non-rotational symmetry. However, other definitions arise to the complexity of the surface description when it comes to on-axis imaging systems, such as Q-type aspheres, spline surfaces, and φ-polynomial surfaces. Freeform optical systems are either designed by direct design approaches [13,15–18] or by using optical surface description techniques [8–10]. Direct design methods are used to calculate the unconstrained optical surfaces to meet the specific optical requirements, and then to fit an initial surface description, which is defined in commercial optical software. The parameters describing the optical surfaces are set to variable in order to find the best optical solution according to the preset merit function. Most of the above works focus on building an unconstrained optical surface. However, the limitation that the unconstrained optical surface must be fitted makes their method very restrictive. Moreover, these methods are more accurate for paraxial approximation. Designing a wide FoV, small f-number, miniature camera lens has been a great challenge and especially difficult for an imaging system with several S-shaped aspheric elements. In contrast, complex mathematic surface description methods allow characterizing any optical surface to realize some particular requirements. The development of manufacturing and measurement techniques had provided a significant step towards the implementation of freeform surfaces in both manufacturing and development. It leads designers to investigate new optical design approaches and affords an alternative approach to the realization of functionalities, such as improved optical performance and package structure. The dependence upon the choice of a potential starting point for the design and the selection of a suitable surface representation is significantly increased with the recent trend of increasing demand for complex imaging systems [19–23]. The common approach in optical design is the use of aspheric surfaces; nevertheless, conventional aspheric surface expression is not optimal because it is not capable of representing extremely aspheric surfaces [24].

To overcome the aforementioned problems, geometric shape modeling ideas and schemes are proposed and implemented to camera lens design. In particular, two quasi-aspheric surface (QAS) representations for S-shaped surfaces by means of pedal and cosine curves seem promising because they are adapted to more closely represent the target surface. The proposed representations are constructed by a polynomial on the base conic function, and an additional truncated sum of basis pedal/cosine function to model a departure from the base conic. The parameterization process on a shape resembling the final form surface is presented using commercial optical design software. Based on the design requirements, a promising starting point using aspheric surfaces is chosen for further system optimization. To verify the feasibility and effectiveness of the proposed method, the representations are implemented during the design process and a least-squares fitting (LSF) algorithm is utilized to obtain a close-fitting QAS profile. Two high-performance design examples that integrate a pedal-based freeform surface and a cosine-based freeform surface are provided, which can offer better performance with large field angle and low distortion.

2. PROBLEM STATEMENT AND QAS DESIGN METHODOLOGY

A. Statement of Problem

Optical systems, such as miniature camera lenses, are traditionally made by assembling several lens elements. The lens elements using S-shaped aspheric surfaces offer an alternative approach for realization of optical components, thus allowing a compact package and superior optical performance as well as acting as a field flattener so that a flat sensor can be used. Many structures have been made to design miniature camera lenses by adopting S-shaped aspheric shapes that have different curvature directions from the center of the surface to the peripheral surface. Patented S-shaped-based embodiments have been analyzed and compared [25–28]. Figure 1 summarizes some existing S-shaped aspheric shapes used to implement miniature camera lenses. Figure 1(a) presents a rotationally symmetric lens where both side surfaces are concave near the vertex and convex in the off-axis zone, which is defined as the concave–convex shape. Figure 1(b) presents a rotationally symmetric lens where both side surfaces are convex near the vertex and concave toward the peripheral FoV. Similarly, it is defined as a convex–concave shape. A rotationally symmetric lens is composed of a convex–concave shape on the left side and a concave–convex shape on the right side, as shown in Figs. 1(c)–1(e). As shown in these figures, besides surface angle, the main difference is the ratio between the central thickness and the edge thickness. The ratio in the case shown in Fig. 1(c) is close to 1, while the ratios in the cases shown in Figs. 1(d) and 1(e) are < 1 and > 1, respectively. Figure 1(f) depicts a rotationally symmetric lens where the left-side surface has a convex–concave-convex shape and the right-side surface has a concave–convex shape. Comparison shows that these aspherical elements are common for correcting aberrations in miniature camera lenses. However, in fact, constructing a random S-shape in a camera lens is a difficult task because the basis of even aspheric terms is not orthogonal, which makes each term variable; a small change in profile may require a positive coefficient on one order offset by a negative coefficient on the next higher order, which leads to large magnitude for

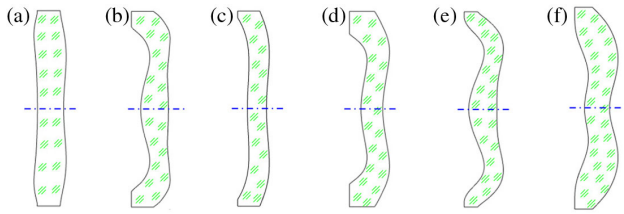

Fig. 1. Comprehensive selection of possible S-shaped aspheric surfaces used to implement the miniature camera lens. (a) Both surfaces have concave-convex shape; (b) both surfaces have convex-concave shape; convex-concave shape on the left-side surface and a concave-convex on the right-side surface while central thickness/edge thickness ratio (c) ≈ 1, (d) <1 and (e) >1; (f) convex-concave-convex shape on the left-side surface and concave-convex shape on the right-side surface.

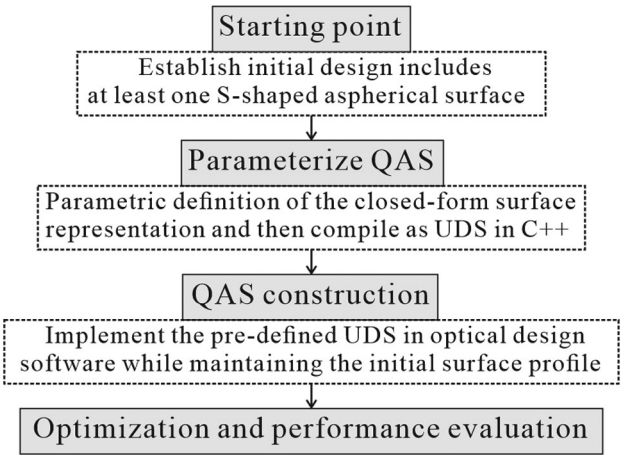

Fig. 2. Flow chart of the optimization design scheme.

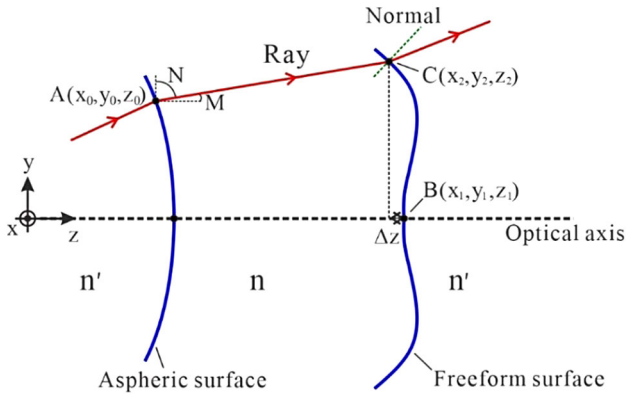

Fig. 3. Schematic drawing of QAS solving method. One ray is traced from left to right.

the conic constant. It is noted that the Forbes Q-polynomials, which are available in commercial optical design software, are orthogonal. The S-shaped surfaces required to achieve stringent optical performance are dramatically more aggressive at the off-axis of the sag departure for the vertex. Furthermore, the optical system is apt to stagnate due to these stringent requirements. To maximize the chances of success in achieving a good solution, a powerful tool is desired, not only to create the required surface shape quickly and easily, but also to escape from stagnation.

B. Design Methodology for QAS

The method we developed for designing freeform optical systems using QAS will be described in this subsection. Figure 2 shows a flow chart of the utilized optimization scheme aiming to completely indicate the optimization principle. The first step is to choose a favorable starting design, which consists at least of an S-shaped aspheric surface. Nevertheless, the generally optical design methods start by investigating an appropriate initial system with full description from a patent library that is close to the target goals. The second step is to parameterize a QAS. The design strategy is to define a representation resembling the final form surface to replace the conventional aspheric surface. This representation can be parametrically described by the function form $z = F(r)$. The overall optical system is set to be symmetrical with respect to the $y-z$ plane. The calculation method of the QAS is illustrated in the schematic diagram in Fig. 3. The simplified pseudocodes of parameterization can be described as

$$\Delta z = \mathrm{SAG} - z_1,$$

$$x_2 = x_0 + \Delta z * L,$$

$$y_2 = y_0 + \Delta z * N,$$

$$z_2 = z_0 + \Delta z * M.$$

In these codes, SAG is the sag of the proposed surface expression that is to evaluate the displacement from the intersection point to the vertex. Δz is the difference of the z value between the intersection point B and the vertex of the proposed surface. (L, N, M) denote the direction cosines of the outgoing ray. The next coordinate of the intersection point $C(x_2, y_2, z_2)$ between the tangent plane of the optical surface and the emitted ray can be solved.

When an oblique ray strikes the surface of different optical properties within the optical system, the ray undergoes reflection and refraction. Therefore, the simple pseudocodes of the calculations are listed below:

$$z' = dz/dr;$$

$$nn = -1/\mathrm{sqrt}(1 + z'^2 * r^2),$$

$$ln = x * z'/\mathrm{sqrt}(1 + z'^2 * r^2),$$

$$mn = y * z'/\mathrm{sqrt}(1 + z'^2 * r^2).$$

In these codes, z' means the derivative of z in the r direction. (nn, ln, mn) indicate the surface normal. Thus, the emitted ray can be calculated based on Snell's law. Specifically, considering an oblique ray on a flat surface, the surface normal can be given by $(nn, ln, mn) = (0, 0, 1)$.

A QAS is programmed using C language and then compiled to a custom dynamic link library (DLL) file to be used by the commercial optical design software. In order to construct an initial structure of QAS and maintain the surface profile, an LSF algorithm can be performed to determine the optimal coefficient values once a close-fitting QAS profile is identified; then the starting point of the optical system with a QAS can be obtained. The last step, the numerical methods of the optical design software optimizer in conjunction with the aberration theory for general optical systems, will be carried out to find the optimal optical performance.

3. DESIGN EXAMPLE AND DISCUSSION

A. Target Specifications and Starting Design Selection

Table 1 lists the target specifications of the camera lens. The wide-angle camera lens is required to provide a FoV around $120° \sim 125°$. If low-light performance is assumed, the lens should have a low f-number of around 2.0. Another major requirement relates to the total length of the optics system. Because of the packaging constraints offered by this lens, its

Table 1. Target Specifications for the Wide-Angle Camera Lens

Parameters	Values
f-number	2.0
Diagonal FoV	120° ∼ 125°
Total length	≤5.5 mm
Working spectrum	486 nm ∼ 656 nm

Table 2. Specifications of the CMOS Sensor for the Wide-Angle Camera Lens

Parameters	Values
Sensor size	1/3.09″
Active area of sensor	4.656 mm × 3.496 mm
Resolution	16.28 megapixels
Pixel size	1.0 μm

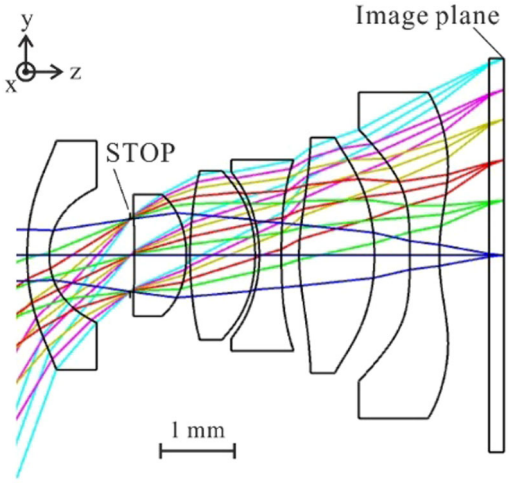

Fig. 4. Optical layout of the starting point of camera lens with one S-shaped element. It consists of all conventional aspheric surfaces in its current form.

length should be limited to less than 5.5 mm, with a back focal length of 0.7 mm from the maximum vertex of the last element to the image plane. A key component of the image capture system is the CMOS sensor, the specifications of which are listed in Table 2. The CMOS used here has a diagonal of 1/3.09 (5.822 mm) with an active area 4.656 mm × 3.496 mm and a resolution of 16.28 megapixels.

Based on the target specifications listed in Table 1, the patent database for the starting point of the camera lens was investigated. Accordingly, the patent CN106646835A was chosen as a starting point [29]. The layout of an enabling starting design of the camera lens is shown in Fig. 4. The initial camera lens has six pieces of plastic aspherical lens, including one S-shaped element. The aperture STOP is located between the first element and the second element. The original camera has an f-number of 2.0, a focal length of 1.96 mm, a full FoV of 140°, an image height of 5.4 mm, and a TTL of 6.5 mm.

B. Design Examples

To demonstrate the superiority of this technology in imaging applications, we realized the miniature camera lenses for two kinds of QAS.

1. Pedal-Based Freeform Camera Lens

Based on the scheme proposed in Subsection 2.B, the main strategy of this section is to present a QAS resembling the form that can be implemented to replace an aspheric surface. Previously, the pedal curve that allows for the representation of an S-shaped characteristic of a lens was introduced [24]. The presented surface representation by superposing the pedal curve is capable of representing an aspherical surface, but the design efficiency is low due to the limitation of variables and lack of conic section by taking the mathematical into account. Based on the features of pedal curves, an improved pedal curve is used to design the camera lens. The highlights of the improved method are its lower complexity, greater efficiency, and flexible variable setting.

The equation of a pedal curve in the $z-y$ plane is given as

$$a^2z^2 + b^2y^2 = \left(z^2 + y^2\right)^2, \tag{1}$$

where a and b are the semimajor axis and semiminor axis of the pedal curve, respectively. As shown in Fig. 5, only the curve along the $+z$ axis is demonstrated. More specifically, the major

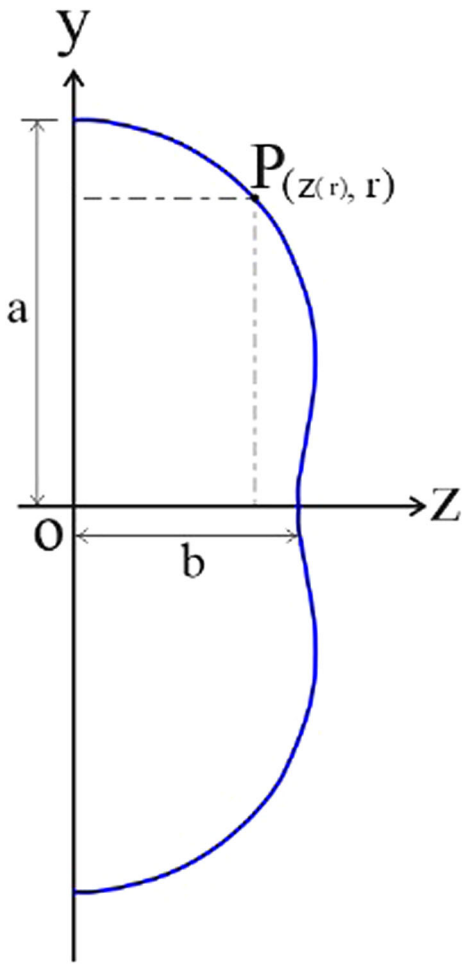

Fig. 5. Schematic diagram of the pedal curve.

a	b	# Terms	1st Order Term	2nd Order Term	3rd Order Term	4th Order Term	5th Order Term	6th Order Term	7th Order Term	8th Order Term
17.5159	6.2133	8.0000	-0.0369	-0.9614	-1.3076	-7.0665	-14.3799	-11.4264	6.1516	8.8285

Fig. 6. Illustration of LDE of ZEMAX with eighth order pedal-based freeform surface.

and minor axes are perpendicular and parallel to the z axis, respectively. Assume that a point on the pedal curve is denoted as $P(z, r)$, where $r = y$ represents the radial distance. Since we are concerned with the distance between the point on the curve and the y axis, z becomes a function of y or r: $z = z(r)$. (z, y) is replaced with (z, r) in Eq. (1); then by solving Eq. (1), the z value as a function of r is given as

$$z = \sqrt{\frac{b^2 - 2r^2 + \sqrt{b^4 + 4\left(a^2 - b^2\right) r^2}}{2}}. \tag{2}$$

From Eq. (2), a general expression of surface sag of the ellipse of the pedal curve can be calculated with Eqs. (3) and (4):

$$S = b - z, \tag{3}$$

$$S = b - \sqrt{\frac{b^2 - 2r^2 + \sqrt{b^4 + 4(a^2 - b^2)r^2}}{2}}, \tag{4}$$

where $r = \sqrt{x^2 + y^2}$ is the radial coordinate of the surface. The conic section is commonly exploited in optical system design due to its special optical property, so the pedal-based freeform surface is represented as a base conic surface with a linear combination of the pedal function. Thus, the pedal-based freeform surface can be expressed in explicit form as follows:

$$z_{(r)} = \frac{cr^2}{1 + \sqrt{1 - (1 + k)c^2 r^2}} + \sum_{i=1}^{n} A_i S^i, \tag{5}$$

where c is the curvature of the base sphere, k is the conic constant that is a function of the eccentricity of the surface, i is the number of terms of the pedal polynomial, and A_i is the ith coefficient of the pedal polynomial. Since the optimization process is performed in commercial optical design software, the proposed pedal-based freeform surface compatible with Zemax OpticStudio is compiled. Figure 6 depicts the lens data editor (LDE), with a pedal-based freeform surface in commercial optical design software. The "# Terms" allows inputting the maximum number of pedal terms; this value may be between 0 and 30, inclusive.

Following the design scheme described in Subsection 2.B, the starting point of the camera lens was optimized using aspheric surfaces for obtaining a good optical performance, and then the S-shaped aspheric surface is further converted to a pedal-based freeform surface one by one, offering reliable convergence during the optimization process. Note that it is practical to keep the similar surface profile on the surface of interest after conversion. To further optimize the system, the surfaces of the first element are also turned into a pedal-based freeform surface representation to help improve the overall optical performance. Benefitting from the implementation of the S-shape at the first

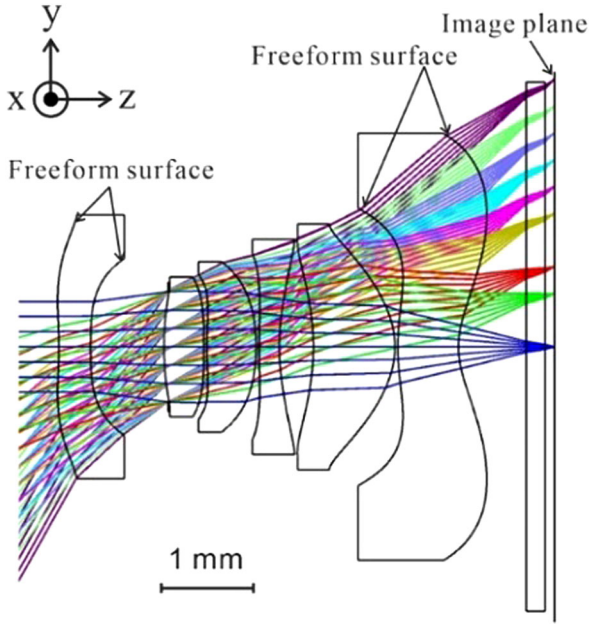

Fig. 7. Optical layout for the pedal-based freeform camera lens.

element, the correction of optical distortion can be further conducted by changing the surface profile. It is indicated that this step of design strategy is very effective in optimizing a freeform camera lens. The layout of the optimized pedal-based freeform camera lens is depicted in Fig. 7. The designed camera lens uses eight aspheric surfaces and four pedal-based freeform surfaces. The diagonal FoV is 121°, f-number is 2.06, and effective focal length is 2.04 mm. The total track of the designed camera lens is about 5.4 mm, which demonstrates the unique behavior of the compact structure. The modulation transfer function (MTF) plots shown in Fig. 8 were evaluated at the spatial frequency of

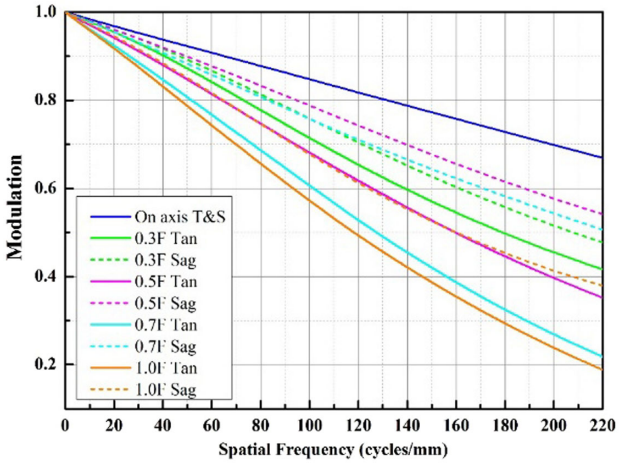

Fig. 8. Polychromatic MTF plots of the pedal-based freeform camera lens.

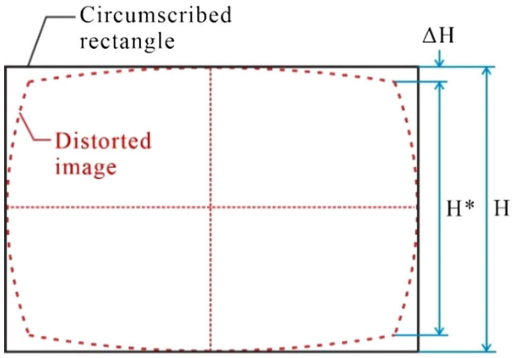

Fig. 9. Definition of the TV barrel distortion.

220 lp/mm, corresponding to a quarter of spatial frequency of the selected CMOS. The polychromatic MTF is above 0.19 at a spatial frequency of 220 lp/mm for all selected field angles.

Both optical distortion and standard mobile imaging architecture television (SMIA-TV) distortion are the key specifications for the image quality evaluation of the wide-angle camera lens. The SMIA-TV distortion evaluation approach was defined by the European Broadcasting Union (EBU). As shown in Fig. 9, the SMIA-TV barrel distortion can be calculated as follows [30]:

$$D_{\mathrm{SMIA}}(\%) = \frac{\Delta H}{0.5H} \times 100 = \frac{(H^* - H)}{H} \times 100, \tag{6}$$

where H is the height of circumscribed rectangle of the distorted image, and H^* is the minimal real image height. The TV distortion grid map is shown in Fig. 10(a). The SMIA-TV distortion is about −13.8% according to Eq. (6). Figure 10(b) shows the optical distortion. We can see that it is well corrected at the central zone. The maximum optical distortion reaches −20.5% at 1.0 field.

2. Cosine-Based Freeform Camera Lens

Considering the camera lens that uses an S-shaped profile as a means to correct distortion, field curvature, and aberrations, a novel geometric shape, referred to as a cosine curve, could be an alternative approach to freeform surface representation. To verify the feasibility of the proposed method that is the relevant S-shaped modeling scheme, simulation and analyses are implemented here.

Compared with the standard aspherical surface, a parametric definition is described for approximating a given optical surface. The general form of the cosine function can be written as

$$z = a[\cos(br)], \tag{7}$$

where $r = \sqrt{x^2 + y^2}$ is the radial surface height, and a and b refer to its amplitude and phase shift, respectively. The parametric definition has the advantage over the standard aspheric definition in terms of the greater extent to which the parametric surface can be created. Therefore, a mathematical representation could be defined as an expansion of a function in a series of cosines, which is given by

$$z = \sum_{i=1}^{n} a_i[\cos^i(b_i r)]. \tag{8}$$

Therefore, the cosine-based freeform surface can be represented as a base conic surface with a linear combination of cosine function. We get

$$z_{(r)} = \frac{cr^2}{1 + \sqrt{1 - (1+k)c^2r^2}} + \sum_{i=1}^{n} a_i[\cos^i(b_i r)]. \tag{9}$$

The definition of conic coefficients in Eq. (9) is identical to the coefficients used in Eq. (5). A similar method is executed in this design case. The QAS based on cosine curve is generated

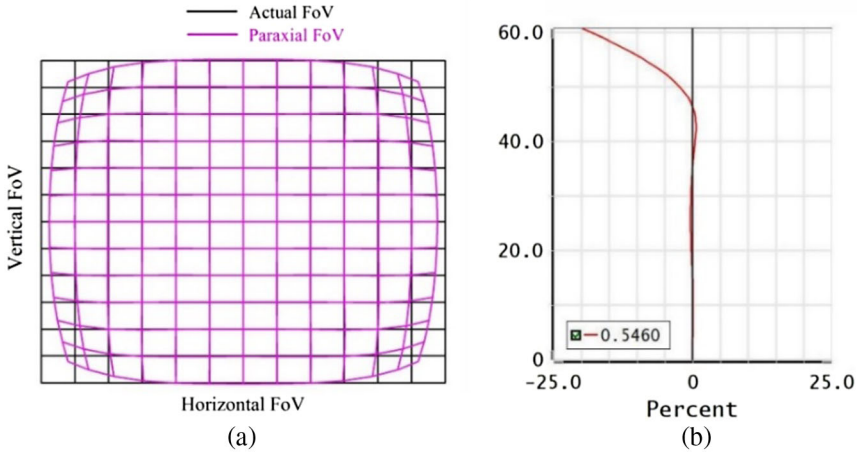

Fig. 10. (a) TV distortion grid map and (b) F-tan(theta) distortion plot for the pedal-based freeform camera lens.

# Terms	a1	b1	a2	b2	a3	b3	a4	b4	a5	b5
5.0000	1.3829	0.8993	-0.2636	1.9230	-1.0291	0.4643	2.9608	0.9513	-3.4677	0.7497

Fig. 11. Example of LDE of ZEMAX with fifth order cosine-based freeform surface.

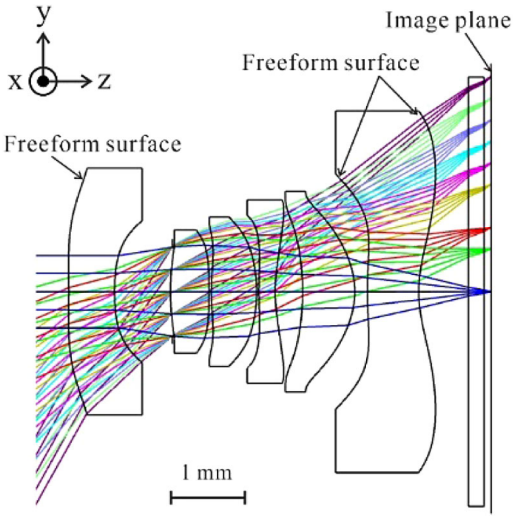

Fig. 12. Optical design layout for the cosine-based freeform camera lens, wherein three freeform surfaces are used.

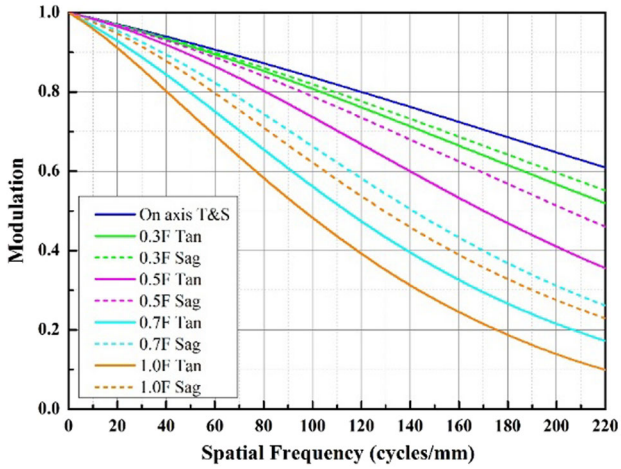

Fig. 13. MTF results for the cosine-based freeform camera lens.

using C language and performed in ZEMAX. The LDE with a cosine-based freeform surface in ZEMAX is given in Fig. 11. The "# Terms" allows the input of the maximum number of cosine terms; this value may be between 0 and 8, inclusive. For cosine-based freeform surface orders $i \leq 8$, the accuracy is sufficient to offer a good performance in imaging optical systems. Moreover, the number of terms is sufficient to decrease the amount of ray-tracing time in the optimization process.

The targeted specifications and starting point are the same as mentioned in Subsection 3.A. The design strategy mentioned above is adopted in the design process. By taking the convergence factor into consideration, we started by converting the aspheric-type surfaces of the last element into a cosine-based freeform surface, and then the aspheric-type surface of the first element was converted to cosine-based freeform surface during the design phase of the intermediate, since optimization using cosine-based freeform surface offers better optical performance. To avoid producing a dramatic deviation error between an aspheric-type surface and a cosine-based freeform surface, a high-precision fitting algorithm is required. We realize a cosine-based freeform camera lens with a 121° diagonal FoV, 2.0 f-number, and a 1.86 mm effective focal length. The final optical design layout for the camera lens using a cosine-based freeform surface is depicted in Fig. 12. The designed camera lens is composed of nine aspheric surfaces and three cosine-based freeform surfaces.

Figure 13 shows the geometric MTF curves for 0, 0.3, 0.5, 0.7, and 1.0 fields in the image space. The MTF values preserves over 0.15 at the designated spatial frequency of 220 lp/mm, except for a peripheral FoV. In addition to the MTF, the same metrics are utilized aiming to characterize the image quality of the camera lens, such as SMIA-TV distortion and optical distortion. Figures 14(a) and 14(b) plot the SMIA-TV distortion grid and optical distortion curve, respectively. The SMIA-TV distortion for the cosine-based freeform camera lens is under −14.2% according to Eq. (6). The distortion curve shows positive values at the midfield. Nevertheless, the maximum distortion is −21.3% at the peripheral field, which is capable of being rectified during image processing.

3. As-Built Performance Evaluation

Because there is a trade-off between production cost and reliability of optical performance, a tolerance analysis should be

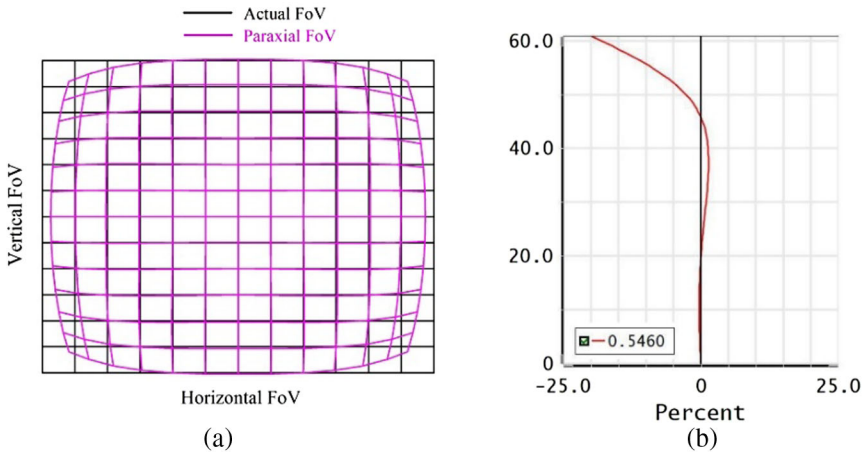

Fig. 14. (a) Distortion grid for full field with cosine-based freeform surfaces; (b) F-Tan(theta) distortion plot for the cosine-based freeform camera lens.

Table 3. Precision Tolerances for Plastic Molded Lens [31]

Tolerance Items	Values
Thickness (μm)	±2
Surface decenter (μm)	±2
Surface tilt (arc min)	1
Element decenter (μm)	±2
Element tilt (arc min)	1
Irregularity (Fr)	1

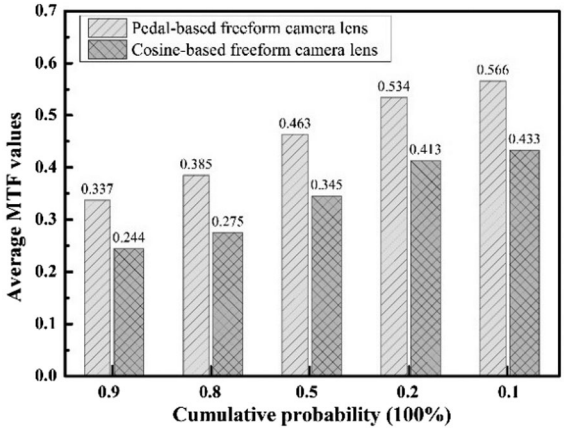

Fig. 15. Cumulative probability obtained from MC simulation.

performed to assess the reliability of optical performance for the designated tolerance allocation to quantify how variations of the surface shape and assembly errors in the manufacturing and assembly processes impact the optical performance. Table 3 lists the tolerance values used in the present design examples. Because of its high accuracy, a Monte Carlo (MC) simulation method is conducted in the tolerance analysis to analyze the nonlinear variations of various manufacturing and assembly errors. In addition, the tangential MTF values measured at a spatial frequency of 110 cycles/mm is employed as a criterion. After running 500 MC trials, the average tangential MTF values are higher than 0.337 and 0.244 at cumulative probabilities of 90% for the pedal-based freeform camera lens and cosine-based freeform camera lens, respectively, as illustrated in Fig. 15. In the case of pedal-based freeform camera lens, the first three parameters for most sensitive tolerances are the surface and element decenter at lens 3 and the element decenter at lens 2. For the cosine-based freeform camera lens, the results illustrate that the surface decenter, the element decenter at lens 2, and the surface decenter at lens 3 are the first three items for most sensitive tolerances.

One way to achieve low-volume, rapid fabrication of lenses, especially freeform lenses, is fabrication directly by means of ultraprecision diamond turning using surface data or a three-dimensional structure. For high-volume production of low-cost products, a complicated fabrication process is required. Therefore, the most popular fabrication method for plastic lenses uses injection molding. However, the proposed QAS representations are uncommon descriptions. It is essential to represent such surfaces in a standard format, such as an even aspheric surface, by approximating them to get adequate surface accuracy. The more coefficients used, the higher is the surface accuracy obtained. In the case of these design examples, the even aspheric surface with maximal 20th order term is capable of accurately approximating QAS without sacrificing their image quality.

C. Comparison of Design Methods

To compare two QAS representations described in the previous section to a more conventional even aspheric surface representation that has been implemented extensively for camera lenses, an additional traditional even aspheric surface representation was performed.

Aiming to provide a fair comparison among these surface representations, the design in Fig. 4 was again utilized as a starting point. The optical system was optimized with the same performance and constraints, as well as an error merit function. The optical performance specification comparison among the three design cases utilizing a pedal-type freeform surface, cosine-type freeform surface, and even aspheric-type surface is presented in Table 4. A suitable surface representation is one of the keys to effectively addressing various problems in design and fabrication. Different surface representation schemes not only lead to different results in convergence studies but also provide different degrees of design freedom. Compared with the cosine-based freeform surface representation approach, the pedal-based

Table 4. Optical Performance Specification Comparison among Three Cases Using Pedal- and Cosine-Based Freeform Surfaces, and Conventional Aspheric Surfaces

Items	Pedal-Based Freeform Camera Lens	Cosine-Based Freeform Camera Lens	Conventional Aspherical Camera Lens
Number of aspheric surfaces	8	9	12
Number of freeform surfaces	4	3	0
Focal length (mm)	2.01	1.82	2.08
f-number	2.07	2.00	2.06
Relative illumination (%)	24	24	26
TTL (mm)	5.4	5.4	5.5
FoV (°)	121.3 × 98.4 × 80.8	121.6 × 99.3 × 80.9	121.1 × 97 × 78.8
CRA at 1.0 F (°)	36.4	37	37
SMIA-TV (%)	−13.8	−14.2	−16.2
Maximum optical distortion (%)	−20.5	−21.3	−23.7

freeform surface representation method demonstrated the ability of getting better optimization convergence. As expected, the pedal-based freeform camera lens and cosine-based freeform camera lenses yield better optical performance in terms of distortion and TTL than aspherical-type camera lenses. Additionally, the pedal and cosine surface type can also offer larger FoV than the conventional aspheric surface type because of the higher degrees of freedom to correct distortion. The CRAs of three design examples are constrained to be less than 37°. The design cases presented above demonstrate that two QAS representation schemes provide a means of empowering the design in an effective way.

4. CONCLUSION

We demonstrate the feasibility of applying geometric shape modeling to represent the freeform surface for designing miniature, low-distortion, and wide-angle camera lenses, especially for mobile phone applications. The representations resembling the S-shaped surfaces, which are conventionally described by an aspheric surface, are exploited. The details of the parameterization process of the design have been explicitly introduced. Two types of new mathematical descriptions of rotationally symmetric QASs that are a critical factor to the effective optical design of the camera lens have been provided. Furthermore, two geometric-shaped modeling strategies and their corresponding two design cases are demonstrated and discussed: pedal-based freeform camera lens and cosine-based freeform camera lens. To verify the effectiveness of the proposed approaches, both the pedal-based freeform camera lens and the cosine-based camera lens are then compared to the design using a conventional aspheric surface. Results show that high image quality of the proposed techniques was demonstrated by the two design examples, which offered lower distortion, larger FoV, smaller TTL, and a higher degree of freedom.

We believe that these geometric shape modeling schemes will provide a valuable inspiration for researchers in designing miniature freeform imaging optics in the future. Our future work will focus on the extension of these design schemes for nonsymmetrical surfaces in imaging applications with well-performing optical systems.

Disclosures. The authors declare no conflicts of interest.

REFERENCES

1. C. Hou, Y. Ren, Y. Tan, Q. Xin, and Y. Zang, "Compact optical zoom camera module based on Alvarez elements," Opt. Eng. **59**, 025104 (2019).
2. W. T. Song, X. M. Liu, Q. J. Cheng, Y. T. Huang, Y. J. Zheng, Y. Liu, and Y. T. Wang, "Design of a 360-deg panoramic capture system based on a smart phone," Opt. Eng. **59**, 015101 (2020).
3. M. J. Sheu, C. W. Chiang, W. S. Sun, J. J. Wang, and J. W. Pan, "Dual view capsule endoscopic lens design," Opt. Express **23**, 8565–8575 (2015).
4. B. Guenter, N. Joshi, R. Stoakley, A. Keefe, K. Geary, R. Freeman, J. Hundley, P. Patterson, D. Hammon, G. Herrera, E. Sherman, A. Nowak, R. Schubert, P. Brewer, L. Yang, R. Mott, and G. McKnight, "Highly curved image sensors: a practical approach for improved optical performance," Opt. Express **25**, 13010–13023 (2017).
5. S. Yokogawa, I. Oshiyama, H. Ikeda, Y. Ebiko, T. Hirano, S. Saito, T. Oinoue, Y. Hagimoto, and H. Iwamoto, "IR sensitivity enhancement of CMOS image sensor with diffractive light trapping pixels," Sci. Rep. **7**, 3832 (2017).
6. J. L. Ruckman, E. M. Fess, and D. Van Gee, "Recent advances in aspheric and conformal grinding at the center for optics manufacturing," Proc. SPIE **3782**, 2–10 (1999).
7. G. W. Forbes, "Characterizing the shape of freeform optics," Opt. Express **20**, 2483–2499 (2012).
8. C. Menke and G. W. Forbes, "Optical design with orthogonal representations of rotationally symmetric and freeform aspheres," Adv. Opt. Technol. **2**, 97–109 (2013).
9. P. Jester, C. Menke, and K. Urban, "B-spline representation of optical surfaces and its accuracy in a ray trace algorithm," Appl. Opt. **50**, 822–828 (2011).
10. K. Fuerschbach, J. P. Rolland, and K. P. Thompson, "A new family of optical systems employing phi-polynomial surfaces," Opt. Express **19**, 21919–21928 (2011).
11. V. Oliker, L. L. Doskolovich, and D. A. Bykov, "Beam shaping with a plano-freeform lens pair," Opt. Express **26**, 19406–19419 (2018).
12. S. L. Wei, Z. B. Zhu, Z. C. Fan, Y. N. Yan, and D. L. Ma, "Double freeform surfaces design for beam shaping with non-planar wavefront using an integrable ray mapping method," Opt. Express **27**, 26757–26771 (2019).
13. Y. Z. Duan, T. Yang, D. W. Cheng, and Y. T. Wang, "Design method for nonsymmetric imaging optics consisting of freeform-surface-substrate phase elements," Opt. Express **28**, 1603–1620 (2020).
14. D. Reshidko and J. Sasián, "Method for the design of nonaxially symmetric optical systems using free-form surfaces," Opt. Eng. **57**, 101704 (2018).
15. Z. Hou, M. Nikolic, P. Benitez, and F. Bociort, "SMS2D designs as starting points for lens optimization," Opt. Express **26**, 32463–32474 (2018).
16. J. C. Miñano, P. Benítez, W. Lin, J. Infante, F. Muñoz, and A. Santamaría, "An application of the SMS method for imaging designs," Opt. Express **17**, 24036–24044 (2009).
17. T. Yang, D. W. Cheng, and Y. T. Wang, "Freeform imaging spectrometer design using a point-by-point design method," Appl. Opt. **57**, 4718–4727 (2018).
18. R. M. Wu, J. Sasián, and R. G. Liang, "Algorithm for designing freeform imaging optics with nonrational B-spline surfaces," Appl. Opt. **56**, 2517–2522 (2017).
19. A. K. Rigler and T. P. Vogl, "Spline function: an alternative representation of aspheric surfaces," Appl. Opt. **10**, 1648–1651 (1971).
20. C. C. Hsueh, T. Elazhary, M. Nakano, and J. Sasian, "Closed-form sag solutions for Cartesian oval surfaces," J. Opt. **40**, 168–175 (2011).
21. J. C. Valencia-Estrada, M. V. Pereira-Ghirghi, Z. Malacara-Hernández, and H. A. Chaparro-Romo, "Aspheric coefficients of deformation for a Cartesian oval surface," J. Opt. **46**, 100–107 (2017).
22. D. W. Cheng, X. J. Chen, C. Xu, Y. Hu, and Y. T. Wang, "Optical description and design method with annularly stitched aspheric surface," Appl. Opt. **54**, 10154–10162 (2015).
23. B. Ma, K. Sharma, K. P. Thompson, and J. P. Rolland, "Mobile device camera design with Q-type polynomials to achieve higher production yield," Opt. Express **21**, 17454–17463 (2013).
24. Y. F. Yan and J. Sasian, "Miniature camera lens design with a freeform surface," Proc. SPIE **10590**, 1059012 (2017).
25. Y. H. Yao, Y. Shinohara, and L. Y. Liao, " Imaging lens system," U.S. patent 20180364457A1 (20 December 2018).
26. S. T. Lai, "Six-piece optical lens system with a wide field of view," U.S. patent 10,175,461B1 (8 January 2019).
27. W. Y. Chen, "Photographing optical lens system, image capturing unit and electronic device," U.S. patent 9,678,315 (13 June 2017).
28. Y. M. Chang, "Optical image capturing system," U.S. patent 10,571,658B2 (25 February 2020).
29. F. J. Dai, "Wide angle camera lens," CN patent 106646835A (10 May 2017).

30. Q. Z. Wang, W. C. Cheng, N. Suresh, and H. Hua, "Development of the local magnification method for quantitative evaluation of endoscope geometric distortion," J. Biomed. Opt. **21**, 056003 (2016).

31. R. Bates, "Performance and tolerance sensitivity optimization of highly aspheric miniature camera lenses," Proc. SPIE **7793**, 779302 (2010).